Supplementary Material for Scaling Laws and Mechanisms of Hydrodynamic Dispersion in Porous Media

Yang Liu[1], Han Xiao[1], Tomás Aquino[2], Marco Dentz[2,*], and Moran Wang[1,*]
[1]*Department of Engineering Mechanics, Tsinghua University, Beijing* 100084*, China*
[2]*Spanish National Research Council (IDAEA-CSIC),* 08034*, Barcelona, Spain*
(Dated: October 26, 2024)

CONTENTS

I. CONTINUOUS TIME RANDOM WALK MODEL

The longitudinal dispersion coefficient is derived from the one-dimensional random walk of particles under Dirac-Delta injection. Particles move between pores through connecting throats, with longitudinal displacement Δx and duration Δt which are random variables characterized by the probability density functions (PDF) $\omega(x)$ and $\psi(t)$, respectively. After n steps, the particle's location and the evolution time are updated like

$$x_{n+1} = x_n + \Delta x_n, \quad t_{n+1} = t_n + \Delta t_n. \tag{S1}$$

The continuous time random walk (CTRW) framework [1] provides the evolution equation of the particle distribution in the form of a partial differential equation as

$$R(x,t) = \int_{-\infty}^{+\infty} dx'\, \omega(x-x') \int_0^t dt'\, \psi(t-t') R(x',t') + \delta(x-x_0)\delta(t), \tag{S2}$$

$$p(x,t) = \int_0^t dt'\, \Psi(t-t') R(x,t'), \tag{S3}$$

$$\Psi(t) = 1 - \int_0^t dt''\, \psi(t''), \tag{S4}$$

where $R(x,t)$ denotes the probability density of a particle reaching location x at time t and $p(x,t)$ represents the concentration. δ denotes the Dirac delta function and x_0 denotes the initial position of particles.

The solution of the concentration in Fourier-Laplace space is given by [1]

$$\tilde{p}^*(k,\lambda) = \frac{1-\psi^*(\lambda)}{\lambda} \frac{1}{1-\tilde{\omega}(k)\psi^*(\lambda)}, \tag{S5}$$

with Fourier and Laplace transforms defined by

* marco.dentz@csic.es
mrwang@tsinghua.edu.cn

$$\tilde{f}(k) = \int_{-\infty}^{+\infty} e^{ikx} f(x) dx, \tag{S6}$$

$$f^*(\lambda) = \int_{0}^{+\infty} e^{-\lambda t} f(t) dt. \tag{S7}$$

Spatial moments $m_1^*(\lambda)$ and $m_2^*(\lambda)$ of the concentration plume in Laplace space are determined as

$$m_1^*(\lambda) = -i \left. \frac{\partial \tilde{p}^*(k,\lambda)}{\partial k} \right|_{k=0}, \quad m_2^*(\lambda) = - \left. \frac{\partial^2 \tilde{p}^*(k,\lambda)}{\partial k^2} \right|_{k=0}. \tag{S8}$$

Substituting equation (S5) into (S8) we obtain

$$m_1^*(\lambda) = v_0 \lambda^{-2} \mathcal{K}^*(\lambda), \tag{S9}$$

$$m_2^*(\lambda) = 2v_0^2 \lambda^{-3} [\mathcal{K}^*(\lambda)]^2 + 2D_0 \lambda^{-2} \mathcal{K}^*(\lambda), \tag{S10}$$

where we define

$$\mathcal{K}^*(\lambda) = \frac{\langle t \rangle \lambda \psi^*(\lambda)}{1 - \psi^*(\lambda)}, \tag{S11}$$

and

$$v_0 = \frac{\langle x \rangle}{\langle t \rangle}, \quad D_0 = \frac{\langle x^2 \rangle}{2\langle t \rangle}, \tag{S12}$$

with the moments defined as

$$\langle t \rangle = \int t \, \psi(t) \, dt, \quad \langle t^2 \rangle = \int t^2 \, \psi(t) \, dt, \tag{S13}$$

and

$$\langle x \rangle = \int x \, \omega(x) \, dx, \quad \langle x^2 \rangle = \int x^2 \, \omega(x) \, dx. \tag{S14}$$

The moments $m_1^*(\lambda)$ and $m_2^*(\lambda)$ at the asymptotic limit ($\lambda \to 0$) are determined by expanding $\mathcal{K}^*(\lambda)$ at the long-time limit [2],

$$\mathcal{K}^*(\lambda) \approx \mathcal{K}^* \Big|_{\lambda=0} + \lambda \frac{d\mathcal{K}^*}{d\lambda} \Big|_{\lambda=0} = 1 + \lambda \mathcal{K}_\infty, \tag{S15}$$

$$\mathcal{K}_\infty = \frac{\langle t^2 \rangle - 2\langle t \rangle^2}{2\langle t \rangle}. \tag{S16}$$

Substituting equations (S15-S16) into (S9) and (S10), respectively, we get

$$m_1^*(\lambda) = v_0 \lambda^{-2} \left(1 + \lambda \mathcal{K}_\infty\right), \tag{S17}$$

$$m_2^*(\lambda) = 2v_0^2 \lambda^{-3} \left(1 + \lambda \mathcal{K}_\infty\right)^2 + 2D_0 \lambda^{-2} \left(1 + \lambda \mathcal{K}_\infty\right). \tag{S18}$$

Inverse Laplace transforms of equations (S17) and (S18) give

$$m_1(t) = v_0 (t + \mathcal{K}_\infty), \tag{S19}$$

$$m_2(t) = v_0^2 (t + \mathcal{K}_\infty)^2 + 2D_0 (t + \mathcal{K}_\infty) + 2v_0^2 \mathcal{K}_\infty t + v_0^2 \mathcal{K}_\infty^2. \tag{S20}$$

The mean square displacement of the concentration plume is

$$\sigma_L^2(t) = m_2(t) - (m_1(t))^2 = 2D_0 (t + \mathcal{K}_\infty) + 2v_0^2 \mathcal{K}_\infty t + v_0^2 \mathcal{K}_\infty^2. \tag{S21}$$

Consequently, the asymptotic dispersion coefficient is calculated as

$$D_L = \frac{1}{2} \frac{d\sigma_L^2(t)}{dt} = D_0 + v_0^2 \mathcal{K}_\infty. \tag{S22}$$

Substituting equation (S12) together with (S16) into (S22), we obtain

$$D_L = \frac{\langle x^2 \rangle}{2\langle t \rangle} + \frac{\langle x \rangle^2}{\langle t \rangle^2} \frac{\langle t^2 \rangle - 2\langle t \rangle^2}{2\langle t \rangle} = \frac{\langle x \rangle^2}{2\langle t \rangle} \left(\frac{\langle t^2 \rangle - \langle t \rangle^2}{\langle t \rangle^2} + \frac{\langle x^2 \rangle - \langle x \rangle^2}{\langle x \rangle^2} \right). \tag{S23}$$

Since $\psi(t)$ generally exhibits a much broader distribution than $\omega(x)$ in porous media implying $\frac{\langle t^2 \rangle - \langle t \rangle^2}{\langle t \rangle^2} \gg \frac{\langle x^2 \rangle - \langle x \rangle^2}{\langle x \rangle^2}$, we approximate the longitudinal dispersion coefficient as

$$D_L \approx \frac{\langle x\rangle^2}{2\langle t\rangle}\frac{\langle t^2\rangle - \langle t\rangle^2}{\langle t\rangle^2}. \tag{S24}$$

We define the global Péclet number as $Pe = \overline{U}\ell/D_m$. $\overline{U}$ denotes the average velocity, which is calculated as the Darcy velocity divided by porosity, and ℓ is the characteristic length, typically taken as the grain size. Equation (S24) highlights the critical role of $\psi(t)$ in the scaling relationship between the dispersion coefficient D_L and the Péclet number Pe. The function $\psi(t)$ characterizes the statistical properties of particle transition times and is influenced by both intra-pore and inter-pore flow variabilities as well as molecular diffusion.

II. GLOBAL DISTRIBUTION OF TRANSITION TIMES

The global PDF $\psi(t)$ of transition times is obtained by marginalization of the joint PDF $\psi_t(t|\tau)\hat{\psi}_\tau(\tau)$,

$$\psi(t) = \int_{\tau_{\min}}^{\tau_{\max}} \psi_t(t|\tau)\hat{\psi}_\tau(\tau)\, d\tau. \tag{S25}$$

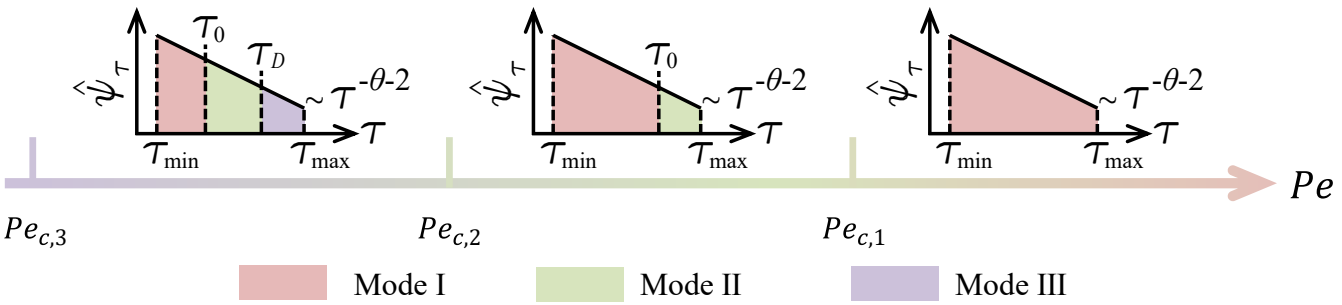

FIG. 1. Schematic of particle transition patterns for networks with large ratios of $\tau_{\max}/\tau_{\min}$. The subfigures of $\hat{\psi}_\tau(\tau)$ are presented in a log-log plot. τ_0 represents the advection time of the tube for which $\tau = \tau_{\mathrm{D,R}}$.

When the ratio $\tau_{\max}/\tau_{\min}$ is large, the transition modes throughout the network can be classified into three patterns based on the global Péclet number Pe, as shown in Figure 1. For simplicity, the characteristic length for Pe is defined as the length of the tube, i.e., $\ell = l$. Furthermore, the average velocity is estimated by taking the mean of the maximum velocities within the pipes, namely, $\overline{U} = \langle v\rangle$. We define $Pe_{\mathrm{c},1}$ and $Pe_{\mathrm{c},2}$ as the minimum Péclet numbers at which the conduit with $\tau_{\max}$ reaches modes I and II, respectively, and $Pe_{\mathrm{c},3}$ as the minimum Péclet number for the conduit with $\tau_{\min}$ as it reaches mode I. These critical Péclet numbers are derived as

$$Pe_{\mathrm{c},1} = \frac{l^2}{R_{\min}^2}\frac{\theta-1}{\theta}\frac{(R_{\max}/R_{\min})^{2\theta}-1}{(R_{\max}/R_{\min})^{2\theta-2}-1}, \tag{S26}$$

$$Pe_{\mathrm{c},2} = \frac{\theta-1}{\theta}\frac{(R_{\max}/R_{\min})^{2\theta}-1}{(R_{\max}/R_{\min})^{2\theta-2}-1}, \tag{S27}$$

$$Pe_{\mathrm{c},3} = \frac{l^2 R_{\min}^2}{R_{\max}^4}\frac{\theta-1}{\theta}\frac{(R_{\max}/R_{\min})^{2\theta}-1}{(R_{\max}/R_{\min})^{2\theta-2}-1}, \tag{S28}$$

if $\theta \neq 1$, and

$$Pe_{\mathrm{c},1} = \frac{l^2}{R_{\min}^2}\frac{(R_{\max}/R_{\min})^2-1}{2\ln(R_{\max}/R_{\min})}, \tag{S29}$$

$$Pe_{\mathrm{c},2} = \frac{(R_{\max}/R_{\min})^2-1}{2\ln(R_{\max}/R_{\min})}, \tag{S30}$$

$$Pe_{\mathrm{c},3} = \frac{l^2 R_{\min}^2}{R_{\max}^4}\frac{(R_{\max}/R_{\min})^2-1}{2\ln(R_{\max}/R_{\min})}, \tag{S31}$$

if $\theta = 1$.

When $Pe > Pe_{\mathrm{c},1}$, all conduits are in mode I. When $Pe_{\mathrm{c},2} < Pe < Pe_{\mathrm{c},1}$, conduits with smaller τ are in mode I while those with larger τ are in mode II, separated by τ_0. When $Pe_{\mathrm{c},3} < Pe < Pe_{\mathrm{c},2}$, the conduits with the smallest

to the largest τ are in mode I, II, and III, separated by τ_0 and τ_{D}, respectively. Here, τ_0 represents the advection time of the tube for which $\tau = \tau_{\mathrm{D,R}}$.

We first consider the scenario with a large ratio $\tau_{\max}/\tau_{\min}$ and $0 < \theta < 1$. When $Pe > Pe_{\mathrm{c},1}$, the transition time PDF $\psi(t)$ is expressed as:

$$\psi(t) = \int_{\tau_{\min}}^{\tau_{\max}} 2\tau^2 t^{-3} H(t-\tau) H(\tau_{\mathrm{B}} - t) C_\tau \tau^{-\theta-2}\, d\tau, \tag{S32}$$

which gives

$$\psi(t) = \begin{cases} \frac{2C_\tau}{-\theta+1} t^{-3} \left(t^{-\theta+1} - \tau_{\min}^{-\theta+1}\right), & t \in [\tau_{\min}, \tau_{\max}], \\ \frac{2C_\tau}{-\theta+1} t^{-3} \left(\tau_{\max}^{-\theta+1} - \tau_{\min}^{-\theta+1}\right), & t \in (\tau_{\max}, \tau_{\mathrm{B}}]. \end{cases} \tag{S33}$$

Given $0 < \theta < 1$, it is evident that $t^{-\theta+1} \gg \tau_{\min}^{-\theta+1}$ for $t \in [\tau_{\min}, \tau_{\max}]$. Thus, equation (S33) can be approximated as

$$\psi(t) = \begin{cases} \frac{2C_\tau}{-\theta+1} t^{-\theta-2}, & t \in [\tau_{\min}, \tau_{\max}], \\ \frac{2C_\tau}{-\theta+1} t^{-3} \left(\tau_{\max}^{-\theta+1} - \tau_{\min}^{-\theta+1}\right), & t \in (\tau_{\max}, \tau_{\mathrm{B}}]. \end{cases} \tag{S34}$$

For $Pe_{\mathrm{c},2} < Pe < Pe_{\mathrm{c},1}$, the transition time PDF $\psi(t)$ is given by

$$\psi(t) = \int_{\tau_{\min}}^{\tau_0} 2\tau^2 t^{-3} H(t-\tau) H(\tau_{\mathrm{B}} - t) C_\tau \tau^{-\theta-2}\, d\tau + \int_{\tau_0}^{\tau_{\max}} \delta(t-2\tau) C_\tau \tau^{-\theta-2}\, d\tau, \tag{S35}$$

which yields

$$\psi(t) = \begin{cases} \frac{2C_\tau}{-\theta+1} t^{-3} \left(t^{-\theta+1} - \tau_{\min}^{-\theta+1}\right), & t \in [\tau_{\min}, \tau_0], \\ \frac{2C_\tau}{-\theta+1} t^{-3} \left(\tau_0^{-\theta+1} - \tau_{\min}^{-\theta+1}\right), & t \in (\tau_0, 2\tau_0], \\ \frac{2C_\tau}{-\theta+1} t^{-3} \left(\tau_0^{-\theta+1} - \tau_{\min}^{-\theta+1}\right) + 2^{\theta+1} C_\tau t^{-\theta-2}, & t \in (2\tau_0, \tau_{\mathrm{B}}], \\ 2^{\theta+1} C_\tau t^{-\theta-2}, & t \in (\tau_{\mathrm{B}}, 2\tau_{\max}]. \end{cases} \tag{S36}$$

Given $0 < \theta < 1$, we obtain $t^{-\theta+1} \gg \tau_{\min}^{-\theta+1}$ and $t^{-\theta-2} \gg t^{-3}$. Since τ_0 represents the maximum value of τ for tubes in mode I, thus, τ_{B}/τ_0 is negligible compared to $\tau_{\max}/\tau_{\min}$. Consequently, within the range $(\tau_0, \tau_{\mathrm{B}}]$, $\psi(t)$ makes a negligible difference and can be approximated by $2^{\theta+1} C_\tau t^{-\theta-2}$. Therefore, equation (S36) can be approximated by

$$\psi(t) \approx \begin{cases} \frac{2C_\tau}{-\theta+1} t^{-\theta-2}, & t \in [\tau_{\min}, \tau_0], \\ 2^{\theta+1} C_\tau t^{-\theta-2}, & t \in (\tau_0, \tau_{\mathrm{B}}], \\ 2^{\theta+1} C_\tau t^{-\theta-2}, & t \in (\tau_{\mathrm{B}}, 2\tau_{\max}]. \end{cases} \tag{S37}$$

Since $\psi(t) \sim t^{-\theta-2}$ consistently across the three subranges, equation (S37) can be further simplified to

$$\psi(t) = C_{\tau,1} t^{-\theta-2}, \quad t \in [\tau_{\min}, 2\tau_{\max}], \tag{S38}$$

where $C_{\tau,1}$ is a normalization constant. For $Pe_{\mathrm{c},3} < Pe < Pe_{\mathrm{c},2}$, the transition time PDF $\psi(t)$ is expressed as

$$\psi(t) = \int_{\tau_{\min}}^{\tau_0} 2\tau^2 t^{-3} H(t-\tau) H(\tau_{\mathrm{B}} - t) C_\tau \tau^{-\theta-2}\, d\tau + \int_{\tau_0}^{\tau_{\mathrm{D}}} \delta(t-2\tau) C_\tau \tau^{-\theta-2}\, d\tau. \tag{S39}$$

With similar derivations from equation (S36-S38), we obtain

$$\psi(t) = C_{\tau,2} t^{-\theta-2}, \quad t \in [\tau_{\min}, \tau_{\mathrm{D}}], \tag{S40}$$

where $C_{\tau,2}$ is a normalization constant.

For the scenario with the large ratio $\tau_{\max}/\tau_{\min}$ and $\theta > 1$, the derivation follows similarly to equations (S32-S40). However, it is crucial to note that $t^{-\theta+1} \ll \tau_{\min}^{-\theta+1}$ and $t^{-\theta-2} \ll t^{-3}$, which contrasts with the case where $0 < \theta < 1$. $\psi(t)$ is derived as

$$\psi(t) = \frac{2C_\tau}{\theta - 1} \left(\tau_{\min}^{-\theta+1} - \tau_{\max}^{-\theta+1}\right) t^{-3}, \quad t \in [\tau_{\min}, \tau_{\mathrm{B}}], \tag{S41}$$

for $Pe > Pe_{\mathrm{c},1}$, and

$$\psi(t) = \begin{cases} \frac{2C_\tau}{\theta-1} \left(\tau_{\min}^{-\theta+1} - \tau_0^{-\theta+1}\right) t^{-3}, & t \in [\tau_{\min}, \tau_{\mathrm{B}}], \\ 2^{\theta+1} C_\tau t^{-\theta-2}, & t \in (\tau_{\mathrm{B}}, 2\tau_{\max}], \end{cases} \tag{S42}$$

for $Pe_{c,2} < Pe < Pe_{c,1}$, and

$$\psi(t) = \begin{cases} \frac{2C_\tau}{\theta-1}\left(\tau_{\min}^{-\theta+1} - \tau_0^{-\theta+1}\right) t^{-3}, & t \in [\tau_{\min}, \tau_B], \\ 2^{\theta+1} C_\tau t^{-\theta-2}, & t \in (\tau_B, \tau_D], \end{cases} \tag{S43}$$

for $Pe_{c,3} < Pe < Pe_{c,2}$.

For the case where $\tau_{\max}/\tau_{\min}$ is large and $\theta = 1$, $\psi(t)$ is derived as

$$\psi(t) = \begin{cases} 2C_\tau t^{-3} \ln\left(t/\tau_{\min}\right), & t \in [\tau_{\min}, \tau_{\max}], \\ 2C_\tau t^{-3} \ln\left(\tau_{\max}/\tau_{\min}\right), & t \in (\tau_{\max}, \tau_B], \end{cases} \tag{S44}$$

for $Pe > Pe_{c,1}$, and

$$\psi(t) = \begin{cases} 2C_\tau t^{-3} \ln\left(t/\tau_{\min}\right), & t \in [\tau_{\min}, \tau_0], \\ 2C_\tau t^{-3} \ln\left(\tau_0/\tau_{\min}\right) + 4C_\tau t^{-3}, & t \in (\tau_0, \tau_B], \\ 4C_\tau t^{-3}, & t \in (\tau_B, 2\tau_{\max}], \end{cases} \tag{S45}$$

for $Pe_{c,2} < Pe < Pe_{c,1}$, and

$$\psi(t) = \begin{cases} 2C_\tau t^{-3} \ln\left(t/\tau_{\min}\right), & t \in [\tau_{\min}, \tau_0], \\ 2C_\tau t^{-3} \ln\left(\tau_0/\tau_{\min}\right) + 4C_\tau t^{-3}, & t \in (\tau_0, \tau_B], \\ 4C_\tau t^{-3}, & t \in (\tau_B, \tau_D], \end{cases} \tag{S46}$$

for $Pe_{c,3} < Pe < Pe_{c,2}$.

To summarize, for a large ratio of $\tau_{\max}/\tau_{\min}$, when $0 < \theta < 1$, $\hat{\psi}_\tau(\tau)$ dominates $\psi(t)$ for $t \le \tau_{\max}$, resulting in $\psi(t) \sim t^{-\theta-2}$, while $\psi_t(t|\tau)$ dominates for $\tau_{\max} < t \le \tau_B$, leading to $\psi(t) \sim t^{-3}$. When $\theta > 1$, $\psi_t(t|\tau)$ dominates $\psi(t)$ for $t \le \tau_B$, resulting in $\psi(t) \sim t^{-3}$, while $\hat{\psi}_\tau(\tau)$ dominates for $t > \tau_B$, leading to $\psi(t) \sim t^{-\theta-2}$.

In the scenario where $\tau_{\max}/\tau_{\min}$ is small, $\hat{\psi}_\tau(\tau)$ is closely approximated by $\delta(\tau - \tau_{\min})$. Particle transitions within throats are almost the same and at mode I. Thus, $\psi(t)$ is given by

$$\psi(t) \approx 2\tau_{\min}^2 t^{-3}, \quad t \in [\tau_{\min}, \tau_B]. \tag{S47}$$

III. THE ASYMPTOTIC DISPERSION COEFFICIENT

The first-order moment $\langle t \rangle$ and the second-order moment $\langle t^2 \rangle$ are determined from equation (S13). The leading-order behavior of $\langle t \rangle$ consistently follows $\langle t \rangle \sim Pe^{-1}$, while the leading-order behaviors of $\langle t^2 \rangle$ vary, as summarized in Table 1 of the main text. The scaling relationships between the hydrodynamic dispersion coefficients D_L and the Péclet number Pe derived from equation (S24) are presented in Table 2 of the main text.

Specially, for the scenario characterized by a large ratio of $\tau_{\max}/\tau_{\min}$ and $0 < \theta < 1$, the expression for $\langle t^2 \rangle$ when $Pe > Pe_{c,1}$ is given by

$$\langle t^2 \rangle = \frac{2C_\tau}{-\theta+1}\left(\tau_{\max}^{-\theta+1} - \tau_{\min}^{-\theta+1}\right)\left(\frac{1}{-\theta+1} + \ln\left(\frac{\tau_B}{\tau_{\max}}\right)\right), \tag{S48}$$

which leads to

$$\langle t^2 \rangle \sim \tau_{\min}^2\left(\frac{1}{-\theta+1} + \ln\left(\frac{\tau_B}{\tau_{\max}}\right)\right) \sim Pe^{-2}\left(\frac{1}{-\theta+1} + \ln\left(\sqrt{\frac{Pe_{t,\min}}{8\eta_{\max}}}\right)\right), \tag{S49}$$

where $Pe_{t,\min}$ and $\eta_{\max}$ represent the local Péclet number and the aspect ratio of the tube with the radius of $R_{\min}$. When $\ln\left(\sqrt{\frac{Pe_{t,\min}}{8\eta_{\max}}}\right) \gg \frac{1}{-\theta+1}$, equation (S49) follows

$$\langle t^2 \rangle \sim Pe^{-2} \ln(Pe), \tag{S50}$$

which subsequently leads to

$$\frac{D_L}{D_m} \sim Pe \ln(Pe). \tag{S51}$$

Otherwise, it follows

$$\langle t^2 \rangle \sim Pe^{-2}, \tag{S52}$$

resulting in

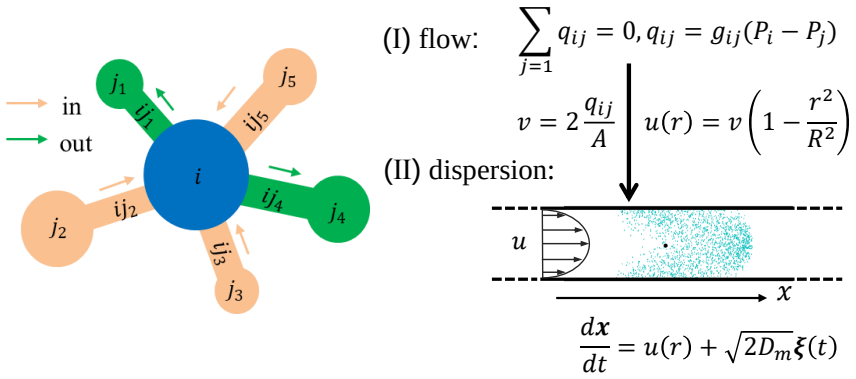

FIG. 2. Schematic of flow and transport between pores and throats in the network model.

$$\frac{D_L}{D_m} \sim Pe. \tag{S53}$$

For a structure characterized by $\theta = 0.8$ and a radius ratio $R_{\max}/R_{\min} = 10$, achieving logarithmic scaling requires a local Péclet number $Pe_{\mathrm{t,min}} > 10^6$, which corresponds to a macroscopic Péclet number $Pe > 10^9$. However, this condition is unattainable under laminar flow, making the observation of logarithmic scaling exceedingly rare in scenarios with a large $\tau_{\max}/\tau_{\min}$ ratio and $0 < \theta < 1$.

IV. NETWORK MODEL FOR FLOW AND DISPERSION

Flow and dispersion through porous media are simulated using network models. The details of the network model for flow and dispersion are outlined below. Figure 2 provides a schematic representation of flow and transport between pores and throats within the network model.

1. Network model for flow

The hydraulic conductance of an individual network element is calculated as

$$g = \frac{k\chi A^2}{\mu l}, \tag{S54}$$

where A is the cross-sectional area, l is the hydraulic conduit length, and μ denotes the fluid viscosity. χ represents the shape factor, and k is a constant dependent on χ. In this study, we consider tubes with circular cross-sections only, where $\chi = 1/4\pi$ and $k = 0.5$. Neighboring pores are connected by three network elements, including the pores located at both ends and the throats between them. The conductance between two adjacent pores is determined by

$$g_{\mathrm{ij}} = \left(g_{\mathrm{i}}{}^{-1} + g_{\mathrm{t}}{}^{-1} + g_{\mathrm{j}}{}^{-1}\right)^{-1}, \tag{S55}$$

where t indicates the throat and i and j represent pores, respectively. The flow rate between pore i and pore j is given by

$$q_{\mathrm{ij}} = g_{\mathrm{ij}}(P_{\mathrm{i}} - P_{\mathrm{j}}), \tag{S56}$$

where P_{i} and P_{j} stand for the pressure in pore i and pore j, respectively. Given a pressure drop between the inlet and outlet of the network, the pressure in pores can be solved by applying mass conservation at each pore. Consider pore i, for instance:

$$\sum_{\mathrm{j}} q_{\mathrm{ij}} = 0. \tag{S57}$$

Subsequently, the pore pressure is substituted into equation (S56) to determine the flow rate q_{ij} in each throat. The velocity profile $u(r)$ within the conduit is determined by Poiseuille law:

$$u(r) = v\left(1 - \frac{r^2}{R^2}\right), \tag{S58}$$

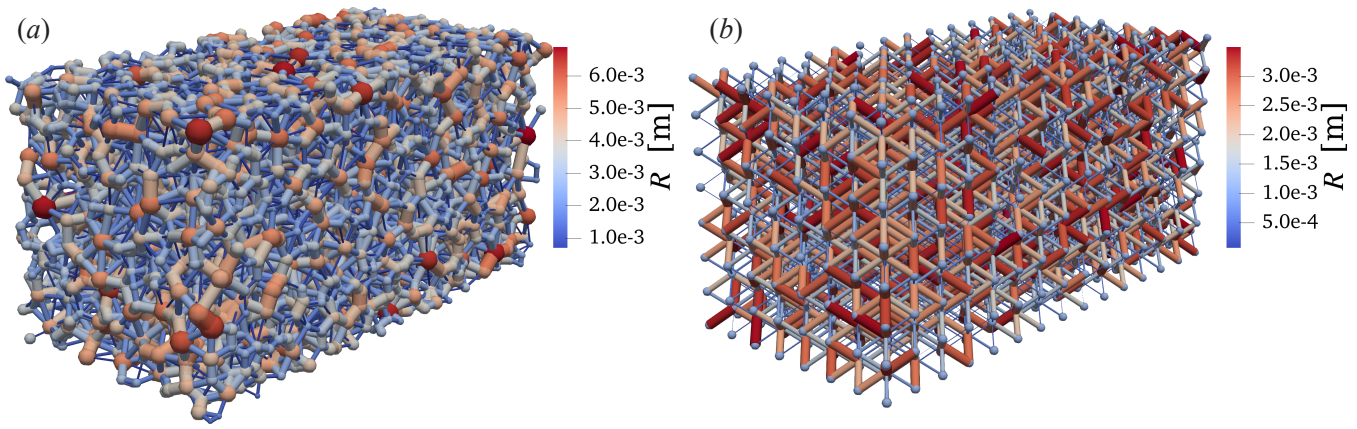

FIG. 3. Illustration of the networks cropped to one-tenth along the longitudinal direction: (a) DN-0.8, a network extracted from a monodisperse sphere pack, and (b) DN-0.5, an artificially generated network with a body-centered cubic (BCC) lattice and varying pore sizes.

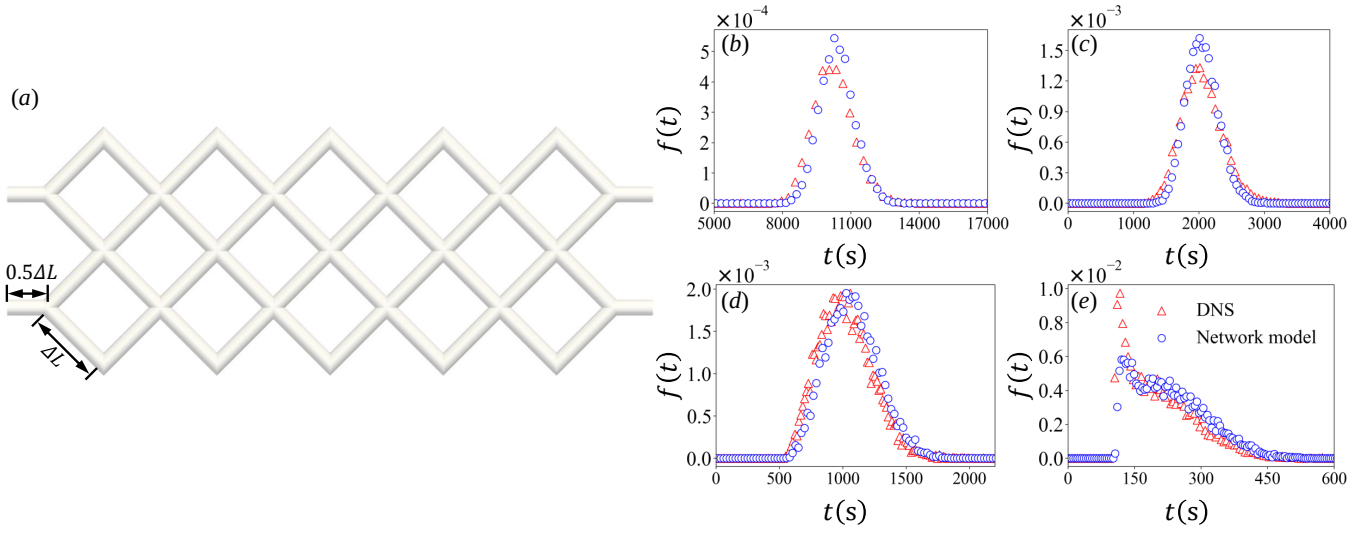

FIG. 4. (a) Illustration of the tube network for validation cases. Comparison of the first-passage time distribution $f(t)$ as predicted by the network model and direct numerical simulation (DNS) for (b) $Pe = 100$, (c) $Pe = 500$, (d) $Pe = 1000$, and (e) $Pe = 5000$.

where r and R denote the radial position and the tube radius, respectively. v represents the maximum velocity within the tube, calculated as $v = 2q_{\mathrm{ij}}/A$.

2. Network model for dispersion

The dispersion of a non-reactive tracer in porous media is modeled using a Lagrangian-based random walk network model. Within the conduits, particles move by advection and diffusion. The particle trajectory is described by the following equation [3]:

$$\frac{d\boldsymbol{x}}{dt} = u(r) + \sqrt{2D_m}\,\boldsymbol{\xi}(t), \tag{S59}$$

where $\boldsymbol{x}$ denotes the particle position and $\boldsymbol{\xi}(t)$ is a unit Gaussian random variable. Here, bold and tilde symbols represent vectors in three-dimensional space.

A bounce-back boundary condition is utilized for diffusion at the walls. In the network model, the redistribution of particles at pore nodes depends on the mechanism of their arrival: advection or diffusion [4]. When a particle enters a pore node during a diffusion step, it is assigned to a new throat based on area-weighted probabilities. Conversely,

when a particle enters a pore node during an advection step, it is assigned to a new throat based on flux-weighted probabilities. This approach contrasts with the theoretical model, which assumes that particle redistribution is exclusively proportional to the flux—a condition that applies only when advection dominates transport globally. To achieve an asymptotic dispersion regime, periodic boundary conditions are implemented, in which particles exiting through the outlet pores are reintroduced at randomly selected inlet pores. The longitudinal dispersion coefficient is determined by the mean square displacement $\sigma_L^2(t)$ with injection time t:

$$D_L = \frac{1}{2}\frac{d\sigma_L^2(t)}{dt}. \tag{S60}$$

Four networks are utilized in the simulation, including three disordered networks (DN-0.5, DN-0.8, and DN-1.1), which have large ratios of $\tau_{\max}/\tau_{\min}$ and corresponding θ values of 0.5, 0.8, and 1.1, respectively, and one ordered network (ON), characterized by a small ratio of $\tau_{\max}/\tau_{\min}$, as illustrated in Figure 3. DN-0.8 is extracted from a monodisperse sphere pack whereas the other networks are artificially generated with a body-centered cubic lattice structure and varying pore size distributions.

3. Validations of the network model

The network model for flow has been thoroughly validated in our previous work [5, 6]. Here we validate the network model for dispersion by examining the transport of solutes through a tube network as depicted in Figure 4(a). The tubes are aligned at an angle of 45° to the mainstream, which flows from left to right. The tubes have a uniform radius R of 0.001 m and an alignment spacing ΔL of 0.01 m.

Various injection rates Q are applied, yielding distinct Péclet numbers defined as $Pe = \overline{U}\Delta L/D_m$, where $\overline{U} = Q/4\pi R^2$ and D_m is the molecular diffusion coefficient with a value of $10^{-9}\,\mathrm{m}^2/\mathrm{s}$. A unit cloud of tracers is released instantaneously at the inlet. An absorbing condition is applied at the outlet, while reflecting conditions are adopted for the rest of the boundaries. The first-passage time distribution $f(t)$ is determined from network simulations and compared with results from direct numerical simulation (DNS).

In the DNS, the flow field is determined using *SimpleFoam*, a flow solver in OpenFOAM, upon which solute transport is simulated via random walk particle tracking. As shown in Figures 4.($b \sim e$), the network model aligns well with the DNS for Pe ranging from 100 to 5000, demonstrating its accuracy and reliability.

[1] B. Berkowitz, A. Cortis, M. Dentz, and H. Scher, Modeling non-fickian transport in geological formations as a continuous time random walk, Rev. Geophys. **44**, RG2003 (2006).

[2] A. Puyguiraud, P. Gouze, and M. Dentz, Pore-scale mixing and the evolution of hydrodynamic dispersion in porous media, Phys. Rev. Lett. **126**, 164501 (2021).

[3] M. Dentz, J. Hidalgo, and D. Lester, Mixing in porous media: concepts and approaches across scales, Transp. Porous Media **146**, 5 (2023).

[4] B. Bijeljic, A. Muggeridge, and M. Blunt, Pore-scale modeling of longitudinal dispersion, Water Resour. Res. **40**, W11501 (2004).

[5] Y. Liu, W. Gong, Y. Zhao, X. Jin, and M. Wang, A pore-throat segmentation method based on local hydraulic resistance equivalence for pore-network modeling, Water Resour. Res. **58**, e2022WR033142 (2022).

[6] Y. Liu, W. Gong, H. Xiao, and M. Wang, A pore-scale numerical framework for solute transport and dispersion in porous media, Adv. Water Resour. **183**, 104602 (2024).